Phosphorous Compounds **Hot Paper**

The Metaphosphite (PO₂⁻) Anion as a Ligand

Josh Abbenseth[+], Florian Wätjen[+], Markus Finger, and Sven Schneider*

Dedicated to Prof. Dr. Wolfgang Kaim on the occasion of his 70th birthday

Abstract: *The utilization of monomeric, lower phosphorous oxides and oxoanions, such as metaphosphite (PO₂⁻), which is the heavier homologue of the common nitrite anion but previously only observed in the gas phase and by matrix isolation, requires new synthetic strategies. Herein, a series of rhenium(I–III) complexes with PO₂⁻ as ligand is reported. Synthetic access was enabled by selective oxygenation of a terminal phosphide complex. Spectroscopic and computational examination revealed slightly stronger σ-donor and comparable π-acceptor properties of PO₂⁻ compared to homologous NO₂⁻, which is one of the archetypal ligands in coordination chemistry.*

The nitrogen oxides NO, NO_2 and N_2O are of high environmental importance as key species in atmospheric nitrogen chemistry.[1] Their extensive use as neutral or charged ligands dates back to the founding days of coordination chemistry and is currently stimulated by biological transformations of the global nitrogen cycle, where the nitrite anion (NO_2^-) stands out as a connecting intermediate.[2,3] In contrast, PO, PO_2 and P_2O are highly reactive species, e.g., as intermediates in the combustion of phosphorous-based flame retardants.[4] For example, the electron affinity of PO_2 (3.4 eV) is close to that of atomic fluorine and strongly exceeds that of NO_2 (2.3 eV).[5] The resulting metaphosphite anion (PO_2^-),[6] which is isoelectronic with SO_2, readily oligomerizes to cyclohexametaphosphite ($P_6O_{12}^{6-}$).[7] Examinations of monomeric lower phosphorous oxides and oxoanions generally require matrix isolation or gas phase techniques.[8] Strategies for controlled access and stabilization are therefore desirable to exploit them as synthetic building blocks.

Lewis-base stabilization was utilized for the isolation of P_2O_4 (Figure 1a) and cationic PO_n^+ ($n = 1, 2$) species.[9,10] In addition, some transition metal clusters with bridging P_xO_y building blocks were reported (e.g. Figure 1b), e.g., via oxygen atom transfer (OAT) reactions to (di-)phosphide

ligands.[8,11] Cummins' PO-complex (Figure 1d) stands out as a unique mononuclear example.[12] The only known PO_2-containing cluster (Figure 1c) features trianionic, side-on bound hypophosphite (PO_2^{3-}).[11b] In contrast, authentic monometaphosphite (PO_2^-) ligands, as phosphorous analogues of the common nitrite anion, remain elusive.

The introduction of 2-phosphaethynolate as P-atom transfer reagent recently gave access to more electron rich (d^2) terminal phosphide complexes, such as [ReP(κ-N^2-PyrPz)(PNP)] (**1**, ᴴPyrPz = 2-(1*H*-pyrazol-5-yl)pyridine, PNP = N(CH₂CH₂P*t*Bu₂)₂; Scheme 1).[13,14] In continuation, we here

[*] Dr. J. Abbenseth,[+] Dr. F. Wätjen,[+] Dr. M. Finger, Prof. Dr. S. Schneider
Universität Göttingen, Institut für Anorganische Chemie
Tammannstrasse 4, 37077 Göttingen (Germany)
E-mail: sven.schneider@chemie.uni-goettingen.de

[+] These authors contributed equally to this work.

Supporting information and the ORCID identification number(s) for the author(s) of this article can be found under:
https://doi.org/10.1002/anie.202011750.

Figure 1. Selected examples of isolable, low-molecular phosphorus oxide compounds (Cp′ = C₅Me₅, Cp″ = 1,3-*t*Bu₂C₅H₃, Dipp = 2,6-*i*Pr₂C₆H₃).
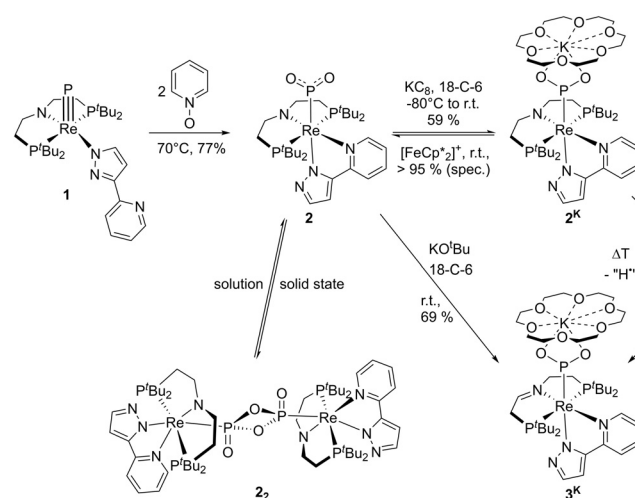
Scheme 1. Synthesis of metaphosphite complexes **2**, **2ᴷ**, and **3ᴷ** via oxygen atom transfer (OAT) to phosphide **1** (Cp* = C₅Me₅).

report OAT reactivity as synthetic entry to lower phosphorous oxide ligands. Facile oxygenation of **1** enabled the synthesis of rhenium(I–III) metaphosphite complexes and examination of M-PO$_2$ bonding.

Heating the terminal phosphide complex **1** in benzene at 70 °C in the presence of pyridine-*N*-oxide results in the formation of a new diamagnetic rhenium species, which could be isolated in 77 % yield (Scheme 1).[15] Full conversion of **1** requires two equivalents of the OAT reagent. Intermediates were not observed. Other OAT reagents like Me$_3$NO or (IMes)N$_2$O (IMes = 3-dimesitylimidazol-2-ylidene)[16] led to unselective decomposition. The product exhibits C_S symmetry on the NMR timescale. The ^{31}P NMR signal of the phosphide-derived fragment (δ_P = 246 ppm) is distinctly upfield shifted with respect to parent **1** (δ_P = 1069 ppm), close to Cummins' PO-complex (Figure 1 d; δ_P = 270 ppm).[12] The ^{1}H NMR spectrum indicates bidentate κ^2-N^1,N^3 coordination of the pyrazolpyridine ligand as judged from comparison with **1** vs. [ReX(PyrPz)(PNP)] (X = I, NCO).[14c] These results support the dioxygenation of the phosphide ligand, which is associated with a rearrangement of the hemilabile PyrPz ligand.

Single crystal X-ray diffraction confirmed phosphide to metaphosphite dioxygenation and crystallization as the dimeric product [(P$_2$O$_4$){Re(PyrPz)(PNP)}$_2$] (**2$_2$**; Figure 2). The bridging μ-P^1,P^2-dimetaphosphite (P$_2$O$_4$$^{2-}$) ligand exhibits a planar P$_2$O$_2$ core with P-O single bonding (1.685(5) Å) and shorter bonds to the terminal oxygen atoms (1.484(5) Å). The bond length of the rhenium ions to the dimetaphosphite P-atoms (2.4564(18) Å) is significantly elongated with respect to parent **1** (Δd = 0.36 Å), in line with reduction of Re-P triple to single bonding. As in solution, the PyrPz ligand of **2$_2$** adopts a κ^2-N^1,N^3 binding mode, which is attributed to reduced σ-donation of bridging P$_2$O$_4$$^{2-}$ vs. P^{3-}. P$_2$O$_4$ was previously observed from P$_2$ oxidation in a cryogenic matrix and could be stabilized with N-heterocyclic carbenes (Figure 1 a).[6e,9,17] In
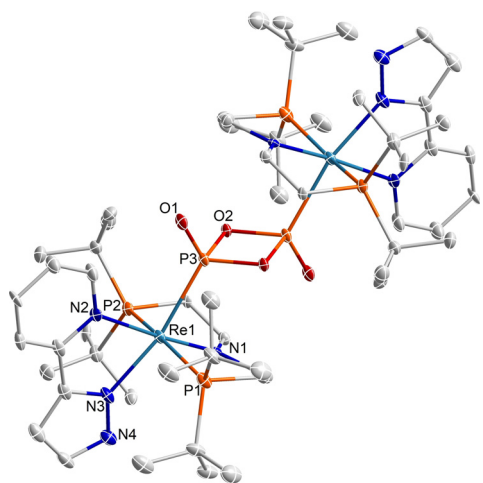
contrast, the dimetaphosphite dianion or its nitrogen analog are unknown.

Interestingly, computational evaluation by density functional theory (DFT) indicated that the equilibrium between monomeric **2** and dimeric **2$_2$** (Scheme 1) is close to thermoneutral.[15,18] ^{31}P NMR chemical shifts were computed to clarify solution speciation. The calculated PO$_2$ chemical shift for monomeric **2** (δ_P(PO$_2$) = 260 ppm, δ_P(PNP) = 46 ppm) distinctly differs from dimeric **2$_2$** (δ_P(P$_2$O$_4$) = 122 ppm, δ_P(PNP) = 43 ppm) and closely resembles the experimental data (δ_P = 246 and 13 ppm). Diffusion coefficients obtained by ^{31}P{^{1}H} DOSY NMR in benzene ($D_{benzene}$ = 7.3 × 10^{-10} m^{2}s^{-1}; r_0 = 4.9 Å) [19] and THF (D_{THF} = 8.1 × 10^{-10} m^{2}s^{-1}, r_0 = 5.9 Å) compare well with related mononuclear complexes, like **1** ($D_{benzene}$ = 7.1 × 10^{-10} m^{2}s^{-1}, r_0 = 5.1 Å), [ReI(PyrPz)(PNP)] ($D_{benzene}$ = 8.4 × 10^{-10} m^{2}s^{-1}, r_0 = 4.3 Å) or [ReCl$_3$(^{H}PNP′)] (D_{THF} = 8.2 × 10^{-10} m^{2}s^{-1}, r_0 = 5.8 Å; ^{H}PNP′ = HN(CH$_2$CH$_2$PiPr$_2$)$_2$) and significantly differ, for example, from the N$_2$ bridged, dinuclear complex [(N$_2$)-{ReCl$_2$(^{H}PNP′)}$_2$] (D_{THF} = 6.4 × 10^{-10} m^{2}s^{-1}, r_0 = 7.5 Å). Despite the large computed chemical shift difference of the mono- and dimetaphosphite ligands ($\Delta\delta_P$ = 138 ppm), the ^{31}P NMR spectra of **2** exhibit negligible temperature dependence ($\Delta\delta_P$(PO$_2$) = 8.0 ppm; $\Delta\delta_P$(PNP) = 5.0 ppm) over a wide range (−80 to +100 °C). Similar invariance was found for variation of the concentration (5–40 mM). The computational and experimental data therefore support that monomeric **2** is the predominant species in solution.

Speciation was further examined by vibrational spectroscopy. The IR spectrum (ATR) of a slowly crystallized, yellowish green solid sample features strong bands at around 550 and 700 cm^{-1} (Figure 3), which can be assigned to in-plane deformation modes of the P$_2$O$_4$-ring of dimeric **2$_2$** by comparison with a computed spectrum (DFT: 526, 704 cm^{-1}). Dissolving this sample in benzene followed by rapid freezing and sublimation of the solvent gives a brown powder, where these signals are absent. Instead, strong bands at 1079 and 1245 cm^{-1} are observed (Figure 3), which are assigned to the symmetric and asymmetric P-O stretching vibrations of a terminal monometaphosphite ligand upon comparison with the computational values for **2** (ν_s = 1086 cm^{-1}, ν_{as} = 1263 cm^{-1}) and reported data for free PO$_2$$^-$ in a KCl matrix (ν_s = 1097 cm^{-1}, ν_{as} = 1207 cm^{-1}), respectively.[6a] These results are in line with solution speciation as monomer **2** vs. crystallization as dimer **2$_2$**. Notably, a solid sample that was obtained from rapid evaporation of a THF/benzene solution showed both sets of signals for the monomer and the dimer (see ESI, Figure S16). In KBr matrix, only the IR signature for **2** was found (Figure S16). This observation might indicate monomer stabilization by interaction of the PO$_2$ ligand with potassium cations, as was found for the anionic rhenium(I) metaphosphite complex **3^K**, which is presented below.

Electrochemical characterization of **2** by cyclic voltammetry (CV) features a reversible one-electron reduction at E_1^0 = −1.81 V (potentials are reported vs. FeCp$_2$$^{+/0}$).[15] Another reduction at very low potential ($E_{2,pc}$ = −2.9 V), which is irreversible at all scan rates (ν = 0.05-3 Vs^{-1}) and associated with an irreversible feature in the reverse scan at

Figure 2. Molecular structure of **2$_2$** in the solid state (thermal ellipsoids set at the 50 % probability level); solvent molecules and hydrogen atoms are omitted for clarity. Selected bond lengths [Å] and angles [°]: Re1–N1 1.900(5), Re1–N2 2.263(5), Re1–N3 2.143(6), Re1–P1 2.4457-(19), Re1–P2 2.4528(18), Re1–P3 2.4564(18), P3–O1 1.484(5), P3–O2 1.685(5); N1-Re1-P3 82.75(16), P1-Re1-P2 163.84(16), O2-P3-O2# 82.8(2).[15]
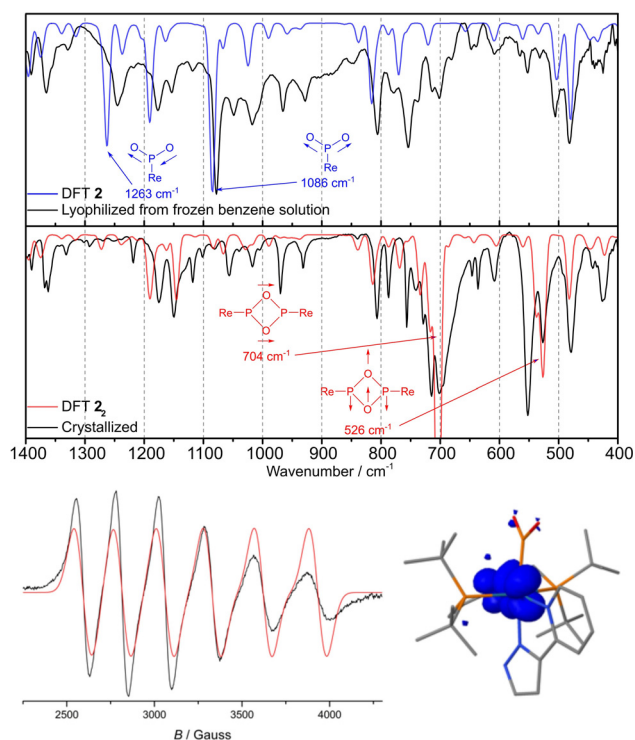
Figure 3. Top: Mid-IR spectra (ATR) of solid **2** and **2₂** obtained by lyophilization of a frozen benzene solution or slow crystallization, respectively, and the computed spectra of **2** (blue) and **2₂** (red) and selected vibrational modes of the {PO₂} moieties. Bottom left: EPR spectrum of **2ᴷ** (THF, 300 K, 9.4169 GHz); simulation parameters: $g_{iso} = 2.046$, $A_{iso}(^{185/187}Re) = 770$ MHz. Bottom right: Computed spin density distribution of **2⁻** (D3BJ-PBE0/def2-TZVP).

$E_{pa} = -1.57$ V, indicates rapid chemical conversion upon overreduction. Controlled potential electrolysis at E_1 over 16 h gave several new features in the CV hinting at slow decomposition of anionic **2⁻**. Chemical reduction was therefore carried out with KC₈/18-C-6 (18-C-6 = 1,4,7,10,13,16-hexaoxacyclooctadecane) to offer a potentially stabilizing counter cation. A distinct color change from red-brown to purple was observed and paramagnetic [K(18-C-6)Re(PO₂)-(PyrPz)(PNP)] (**2ᴷ**; Scheme 1) could be isolated in 59% yield. Near quantitative re-oxidation of **2ᴷ** was obtained with [FeCp*₂][Al{OC(CF₃)₃}₄]. The EPR spectrum of **2ᴷ** at room temperature in solution (Figure 3) exhibits a 6-line signal, which could be satisfactorily simulated with $g_{iso} = 2.046$ and large hyperfine interaction (HFI) with a single low-spin rhenium(II) ion ($A_{iso}(^{185/187}Re) = 770$ MHz).[20] The absence of resolved ³¹P HFI suggests little spin delocalization onto the metaphosphite ligand.[21,22] DFT computations confirm this notion locating the spin density mainly at the rhenium (59%) and pincer nitrogen (30%) atoms (Figure 3). This distribution resembles the computed SOMO of **2⁻** and the LUMO of **2** (Figure 5), which are orthogonal to the Re-PO₂ σ- and π-interactions (see below) and feature predominant Re-N π*-character.

At room temperature, **2ᴷ** decays over several days in solution, which prevented crystallographic characterization. As one of several products, the rhenium(I) metaphosphite

complex **3ᴷ** (Scheme 1) was obtained with an imine pincer ligand that results from formal hydrogen atom loss. Alternatively, **3ᴷ** is easily prepared by deprotonation of parent **2** with KOᵗBu in the presence of 18-C-6 (Scheme 1). The ¹H NMR spectrum of **3ᴷ** confirms C_1 symmetry on the NMR timescale and the presence of an imine group ($\delta_H = 7.86$ ppm). The ³¹P{¹H} NMR signal at $\delta_P(PO_2) = 273$ ppm indicates that the monometaphosphite ligand is preserved. The solution structural assignment was corroborated by single crystal X-ray diffraction (Figure 4), which features **3ᴷ** as contact ion pair with a trigonal-planar PO₂⁻ anion that is κ(P)-bound to rhenium and κ(O,O′)-coordinated to the potassium counter cation. The P−O bond lengths (1.517(2)/1.512(2) Å) resemble those of free PO₂⁻ in the gas phase (1.50(1) Å).[5b] Comparison with Lewis-base stabilized PO₂⁺ species (1.46–1.47 Å)[10b–c] points at weaker P−O bonding in the anion. In turn, the reported PO₂³⁻ ligand (Figure 1c) features one considerably longer, bridging P−O bond (1.58-(3) Å).

The considerably shorter Re-PO₂ bond length of **3ᴷ** (2.2545(7) Å) with respect to dimeric **2₂** (2.4564(18) Å) reflects the lower phosphorous coordination number but might also indicate some Re→PO₂ π back-bonding contribution to the monometaphosphite ligand. For the nitrite homologue, haem-based nitrite reductase activity was associated with Fe→NO₂ π back-bonding in the nitro binding mode.[3c,e,23] Donation into the N-O π-antibonding LUMO of NO₂ results in a redshift of the symmetric NO₂ stretching vibration of, e.g., around $\Delta\nu_s(NO_2) \approx 60$ cm⁻¹ for a low-spin {Feᴵᴵᴵ/ᴵᴵ(NO₂)} redox couple.[3c] The same trend was found for the rhenium(III-I) metaphosphite complexes **2/2ᴷ/3ᴷ**. Reduction of **2** to **2ᴷ** is also associated with a bathochromic shift of $\Delta\nu_s(PO_2) = 60$ cm⁻¹. A smaller shift was found for **2ᴷ** vs. **3ᴷ** ($\Delta\nu_s(PO_2) \leq 17$ cm⁻¹). However, the lower formal metal oxidation state coincides with the replacement of a π-donor
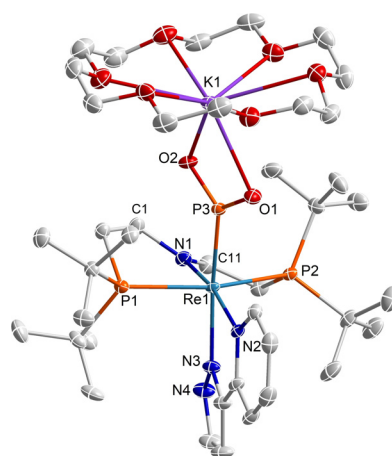

Figure 4. Molecular structure of **3ᴷ** in the solid state (thermal ellipsoids set at the 50% probability level); solvent molecules and H atoms are omitted for clarity. Selected bond lengths [Å] and angles [°]: Re1–N1 2.082(2), Re1–N2 2.141(2), Re1–N3 2.162(2), Re1–P1 2.3977-(7), Re1–P2 2.4332(7), Re1–P3 2.2545(7), N1–C1 1.468(4), N1–C11 1.327(4), P3–O1 1.517(2), P3–O2 1.512(2), O1–K1 2.730(2), O2–K1 2.731(2); N1-Re1-P3 94.31(9), P1-Re1-P2 155.70(2), O1-P3-O2 110.26-(12).[15]

(amide) by a competing π-acceptor (imine) ligand, which precludes direct comparison.

In the MO scheme of **2** (Figure 5), Re→PO_2 back bonding is reflected by the HOMO-1, which features contributions with P-O π-antibonding character. Bonding of the metaphosphite ligand to the metal was further examined by natural bond orbital (NBO) analysis.[15,24] The Re-PO_2 interaction is dominated by the σ-bonding natural localized molecular orbital (NLMO), which is slightly polarized towards phosphorus (**2**: 36% Re, 61% P; **2⁻**: 35% Re, 62% P), yet more covalent with respect to the computed nitro analogue [Re(κ-N-NO_2)(κ-N^2-PyrPz)(PNP)] (**2^{NO2}**: 21% Re, 78% N). Re→PO_2 back donation in **2** is expressed by small contributions (approx. 3%) of the metaphosphite ligand to the NLMOs that represent the two occupied metal d orbitals. The energetic stabilization due to this donor-acceptor π-interaction (ΔE_π) can be estimated by second order perturbation theory within the NBO scheme.[25] A cumulative stabilization energy for π donation from the Re lone pairs of **2** into the metaphosphite π-orbitals of $\Delta E_\pi = 17$ kcal mol⁻¹ was obtained. As expected, the free anion **2⁻** exhibits slightly increased Re→PO_2 back bonding ($\Delta E_\pi = 23$ kcal mol⁻¹). For the nitro complex **2^{NO2}**, $\Delta E_\pi = 21$ kcal mol⁻¹ was computed indicating that the nitro ligand bound to the {Re(PyrPz)(PNP)} fragment is only a slightly stronger π-acceptor than metaphosphite.

In summary, oxygenation of the terminal rhenium phosphide complex **1** gave access to a series of complexes with the unknown metaphosphite (PO_2^-) ligand, that is, the phosphorous analogue of the biologically important nitrite anion. In the solid state, the rhenium(III) compound **2** also exists as dimer **2₂** with a bridging $P_2O_4^{2-}$ dianion. Facile synthesis of rhenium(II) and rhenium(I) complexes by reduction and pincer deprotonation, respectively, demonstrates the chemically robust nature of the metaphosphite ligand. Vibrational
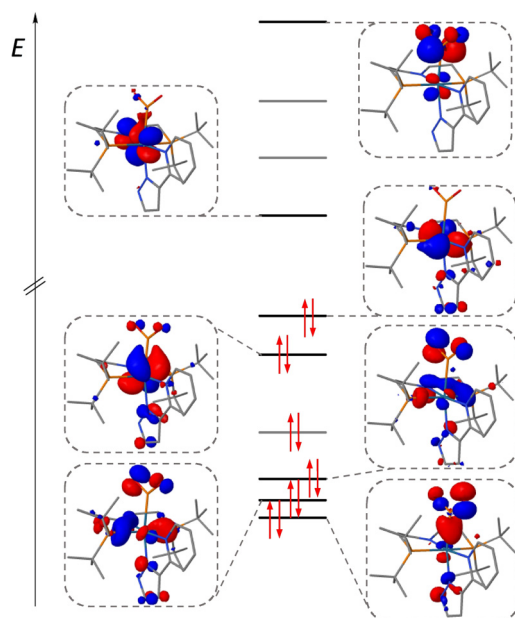
spectroscopy data and computational analysis indicate that the P-bound metaphosphite ligand is a slightly stronger σ-donor and comparable π-acceptor ligand compared with the nitrite homologue.

Conflict of interest

The authors declare no conflict of interest.

[1] S. Manahan, *Environmental Chemistry*, CRC, Boca Raton, FL, **2017**.

[2] A. Werner, *Ber. Dtsch Chem. Ges.* **1907**, *40*, 765.

[3] a) M. A. Hitchman, G. L. Rowbottom, *Coord. Chem. Rev.* **1982**, *42*, 55; b) B. Richter-Addo, P. Legdzins, *Metal Nitrosyls*, Oxford University Press, New York, **1992**; c) G. R. A. Wyllie, W. R. Scheidt, *Chem. Rev.* **2002**, *102*, 1067; d) L. B. Maia, J. J. G. Moura, *Chem. Rev.* **2014**, *114*, 5273; e) A. J. Timmons, M. D. Symes, *Chem. Soc. Rev.* **2015**, *44*, 6708; f) K. J. Koebke, V. L. Pecoraro, *ACS Catal.* **2018**, *8*, 8046.

[4] a) B. Schartel, *Materials* **2010**, *3*, 4710; b) S. Liang, P. Hemberger, M. Steglich, P. Simonetti, J. Levalois-Grützmacher, S. Grützmacher, S. Gaan, *Chem. Eur. J.* **2020**, *26*, 10795.

[5] a) K. M. Ervin, J. Ho, W. C. Lineberger, *J. Phys. Chem.* **1988**, *92*, 5405; b) C. Xu, E. de Beer, D. M. Neumark, *J. Chem. Phys.* **1996**, *104*, 2749; c) C. Blondel, C. Delsart, F. Goldfarb, *J. Phys. B* **2001**, *34*, L281.

[6] a) S. J. Hunter, K. W. Hipps, A. H. Francis, *Chem. Phys.* **1979**, *39*, 209; b) J. S. Ogden, S. J. Williams, *J. Mol. Struct.* **1982**, *80*, 105; c) L. Andrews, R. Whitnall, *J. Am. Chem. Soc.* **1988**, *110*, 5605; d) P. A. Hamilton, *J. Chem. Phys.* **1987**, *86*, 33; e) Z. Mielke, M. McCluskey, L. Andrews, *Chem. Phys. Lett.* **1990**, *165*, 146; f) H. B. Qian, P. B. Davies, I. K. Ahmad, P. A. Hamilton, *Chem. Phys. Lett.* **1995**, *235*, 255.

[7] a) B. Blaser, K.-H. Worms, *Z. Anorg. Allg. Chem.* **1959**, *300*, 237; b) B. Lüer, M. Jansen, *Z. Anorg. Allg. Chem.* **1991**, *601*, 51.

[8] B. T. Sterenberg, L. Scoles, A. J. Carty, *Coord. Chem. Rev.* **2002**, *231*, 183.

[9] Y. Wang, Y. Xie, P. Wie, H. F. Schaefer III, P.v.R. Schleyer, G. H. Robinson, *J. Am. Chem. Soc.* **2013**, *135*, 19139.

[10] a) R. Weiss, S. Engel, *Angew. Chem. Int. Ed. Engl.* **1992**, *31*, 216; *Angew. Chem.* **1992**, *104*, 239; b) P. Rovnaník, L. Kapička, J. Taraba, M. Černík, *Inorg. Chem.* **2004**, *43*, 2435; c) J. Zhou, L. L. Liu, L. L. Cao, D. W. Stephan, *Angew. Chem. Int. Ed.* **2019**, *58*, 18276; *Angew. Chem.* **2019**, *131*, 18444.

[11] a) O. J. Scherer, S. Weigel, G. Wolmershäuser, *Angew. Chem. Int. Ed.* **1999**, *38*, 3688; *Angew. Chem.* **1999**, *111*, 3876; b) A. S. Pronin, A. I. Smolentsev, S. G. Kozlova, I. N. Novozhilov, Y. V. Mirnov, *Inorg. Chem.* **2019**, *58*, 7368.

Figure 5. Molecular orbital scheme of **2** (D3BJ-PBE0/def2-TZVP). For simplicity, pure pyrazolpyridine ligand based π-type orbitals are not displayed.

[12] M. J. A. Johnson, A. L. Odom, C. C. Cummins, *Chem. Commun.* **1997**, 1523.

[13] J. M. Goicoechea, H. Grützmacher, *Angew. Chem. Int. Ed.* **2018**, *57*, 16968; *Angew. Chem.* **2018**, *130*, 17214.

[14] a) M. Joost, W. J. Transue, C. C. Cummins, *Chem. Commun.* **2017**, *53*, 10731; b) J. A. Buss, P. H. Oyala, T. Agapie, *Angew. Chem. Int. Ed.* **2017**, *56*, 14502; *Angew. Chem.* **2017**, *129*, 14694; c) J. Abbenseth, M. Diefenbach, A. Hinz, L. Alig, C. Würtele, J. M. Goicoechea, M. C. Holthausen, S. Schneider, *Angew. Chem. Int. Ed.* **2019**, *58*, 10966; *Angew. Chem.* **2019**, *131*, 11082.

[15] See the Supporting Information (ESI) for synthetic, spectroscopic, crystallographic and computational details. Deposition Numbers 2024567 (for **2₂**) and 2024610 (for **3ᴷ**) contain the supplementary crystallographic data for this paper. These data are provided free of charge by the joint Cambridge Crystallographic Data Centre and Fachinformationszentrum Karlsruhe Access Structures service www.ccdc.cam.ac.uk/structures.

[16] A. G. Tskhovrebov, B. Vuichoud, E. Solari, R. Scopelliti, K. Severin, *J. Am. Chem. Soc.* **2013**, *135*, 9486.

[17] a) M. McCluskey, L. Andrews, *J. Phys. Chem.* **1991**, *95*, 2988; b) C. W. Bauschlicher, M. Zhou, L. Andrews, *J. Phys. Chem. A* **2000**, *104*, 3566.

[18] The stabilization of the singlet state of **2** ($\Delta G^0_{\text{S-T}} = 12.0$ kcal mol^{-1}) is attributed to strong N→Re$^{\text{III}}$ π-donation.

[19] Hydrodynamic radii (r_0) were estimated via the Stokes-Einstein equation.

[20] T. D. Lohrey, G. Rao, D. W. Small, E. T. Oulette, R. G. Bergman, R. D. Britt, J. Arnold, *J. Am. Chem. Soc.* **2020**, *142*, 13805.

[21] a) U. Abram, A. Voigt, R. Kirmse, K. Ortner, R. Hübener, R. Carballo, E. Vasquez-Lopez, *Z. Anorg. Allg. Chem.* **1998**, *624*, 1662; b) F. Ehret, M. Bubrin, S. Záliš, W. Kaim, *Angew. Chem. Int. Ed.* **2013**, *52*, 4673; *Angew. Chem.* **2013**, *125*, 4771.

[22] J. Abbenseth, D. Delony, M. C. Neben, C. Würtele, B. de Bruin, S. Schneider, *Angew. Chem. Int. Ed.* **2019**, *58*, 6338; *Angew. Chem.* **2019**, *131*, 6404.

[23] D. Bykov, F. Neese, *Inorg. Chem.* **2015**, *54*, 9303.

[24] F. Weinhold, C. R. Landis, *Valency and Bonding: A Natural Bond Orbital Donor-Acceptor Perspective*, Cambridge University Press, Cambridge, **2005**.

[25] T. Leyssens, D. Peeters, A. G. Orpen, J. N. Harvey, *Organometallics* **2007**, *26*, 2637.

23578   www.angewandte.org

© 2020 The Authors. Published by Wiley-VCH GmbH

Angew. Chem. Int. Ed. **2020**, *59*, 23574–23578